Parameter Deviation Effect Study of the Power Generation Unit on a Doubly-Fed Induction Machine-based Shipboard Propulsion System

Kai Ni, *Member, IEEE*, Yihua Hu, *Senior Member, IEEE*, and Chun Gan, *Member, IEEE*

Abstract— To lower the difficulty of fault protection, a doubly-fed induction machine based shipboard propulsion system (DFIM-SPS) that is partially power decoupled is presented. In such an intrinsically safe SPS architecture, a synchronous generator (SG) is employed for power generation, and the accuracy of the parameters of power generation unit (PGU) plays an important role in SPS stable operation. In this paper, the PGU parameter deviations are studied to evaluate the effects on system performance. The models of salient-pole SG, type DC1A excitation system (EXS) and DFIM are illustrated first. Besides, the corresponding control scheme is explained. For the 16 important parameters of PGU, up to 40% of parameter deviations are applied to implement parameter sensitivity analysis. Then, simulation studies are carried out to evaluate the parameter deviation effects on system performance in detail. By defining three parameter deviation effect indicators (PDEIs), the effects on the PGU output variables, which are the terminal voltage and output active power, are studied. Moreover, the increasing rates of PDEIs with different degrees of parameter deviations for the key parameters are analyzed. Furthermore, the overall system performance is investigated for the two most influential PGU parameters. This paper provides some vital clues on SG and EXS parameter identification for DFIM-SPS.

Index Terms—shipboard propulsion system, partially power decoupled, doubly-fed induction machine, synchronous generator, parameter deviation

Nomenclature

V, I, E	Constant values of voltage, current, internal voltage
v, i, φ, f	Instantaneous values of voltage, current, flux, frequency
P, Q, PF	Active power, reactive power, power factor
L_{ls}, L_{lr}	Stator and rotor leakage inductance
L_{ss}, L_s, L_r	Inductances on the source side converter, stator, rotor ($L_s = L_m + L_{ls}$; $L_r = L_m + L_{lr}$)
S, u	Switching signal, control signal
v_f, v_{f0}	Field voltage, initial field voltage
X, Z	Reactance, impedance
R, L, C	Resistance, inductance, capacitance
$\theta_\varphi, \theta_e, \theta_m, \theta_{slip}$	Flux angle, synchronous angle, rotor angle, slip angle
$\omega_e, \omega_m, \omega_r$	Synchronous angular frequency, mechanical rotor angular speed, electrical rotor angular speed
T_{em}, T_L	Electromagnetic torque and load torque
n_p, H, F	Number of pole pairs, inertia constant, friction factor
p	Differential calculator d/dt
v_f, v_k	Field and damping voltages
V_{stab}	Stablizing voltage
K_a, K_e, K_f, K_d	Regulator, exciter, stabilizer gains, damping factor
k_s, k_p, k_i	Stator coupling factor, proportional gain, integral gain
X_m, X_l, X_k	Mutual leakage and damping reactance
T_d, T_{do}, T_{kd}	d-axis short-circuit, open-circuit and damping time constants
T_q, T_{qo}	q-axis short-circuit and open-circuit time constants
T_a, T_e, T_f, T_r	Time constants for regulator, exciter, stabilizer, and low-pass filter
R_{mtr}, L_{mtr}	Transformer magnetization resistance and inductance
PWM, LPF	Pulse width modulation, low-pass filter
Subscripts	
s, r, ss, t	Stator-side, rotor-side, source-side, total variables
$0, o$	Initial and open-circuit variables
n	Nominal values
f, k, T	Field winding, damper winding, terminal variables
ref	Reference value
a, b, c	Phases A, B, C
com, SG	Variables for compensator and sychronous generator
dc	DC-bus variables
$\alpha, \beta/d, q$	Direct and quadrature components referred to the stationary/synchrnous reference frame
Superscripts	
'	Transient variables
''	Sub-transient variables

*Note: The variables defined for DFIM are not specified.

I. Introduction

NOWADAYS, power electronic interfaces are extensively applied for all-electric ships to enhance the controllability of shipboard power system (SPS) [1]. Therefore, DC SPSs develop fast in recent years [2-4]. Nevertheless, the dominant status of power electronic devices in DC power transmission based SPS threatens the system reliability due to the easy-to-breakdown feature [5], and high difficulty of DC power system fault protection is unavoidable [6-8]. Besides, in the case of large-scale power conversion modules, usually the DC-bus voltage can be high that presents potential safety hazards [9]-[12].

Since doubly-fed induction machines (DFIMs) are capable of variable-speed constant-frequency operation, bidirectional power flows and small power converter volume, they have been widely used in wind turbines [13]. DFIM functions as the bridge between squirrel cage induction machines [14] and synchronous machines [15]. Such a kind of multiport electrical machine is endowed with high power rating, high fault tolerance, and strong power flow control capability [16], making it attractive for SPS applications [17, 18].

A DFIM-based power system without power electronic converter on the stator side is partially power decoupled. There are two paths for power flows, namely the direct and power electronic paths for the stator and rotor of DFIM, respectively. Only the slip power is controlled by using a back-to-back power converter (BTBPC) to minimize the volume of on-board integrated power electronics. However, compared with the application of DFIM in wind energy conversion systems, a much wider range of rotor speed is required for a propulsion system. In this case, a number of research activities that modify the conventional DFIM-based power system structure for SPS application were carried out [19]-[24].

In order to achieve the full speed range, the commonly adopted method is applying an additional power inverter for the stator side of DFIM [19]-[22]. Although reliable operation of DFIM propulsion systems is achieved by the aforementioned solutions with a full speed range, the intrinsic strength of a DFIM-based power system of small converter volume is lost. To retrieve the advantage of controlling the SPS with reduced power electronics and obtaining the full speed range simultaneously, the concept of "switched doubly fed machine" (switched DFM) was proposed in [23]. The design process was discussed for a switched DFM drive in [23], then the control architecture was investigated in [24] to realize the seamless transition between the two operation modes to minimize the volume of power electronics.

The power supply onboard a DFIM-SPS is mainly provided by the power generation unit (PGU) composed of a synchronous generator (SG) and its excitation system (EXS). Because of aging of power components and high temperature, the variations in SG parameters may occur, which can seriously deteriorate the system performance. In addition, the parameter deviations of the EXS also influence the overall system performance. According to the authors' knowledge, none of the previous research on DFIM considered the PGU based on SG for propulsion system power supply, not to mention the effects of parameter deviations of PGU on system performance.

The fundamental concepts of synchronous machine (SM) stability were investigated in detail by taking the effects of excitation control into account in [25], which provided guidance for the research in SM-based power systems. In addition, based on the study of modelling process without simplifications, a method that determines the SM parameters was proposed in [26]. On top of that, to ease the computational burden, some techniques with necessary simplifications were developed for the sake of exploring SM-based power system transients [27]-[29]. In order to provide satisfactory voltage control performance for an SG when there are uncertainties in

the system operating conditions [30] and exciter parameters [31], several design approaches for EXS were proposed. In [32], online calibration of sensorless position estimation was implemented by considering parametric uncertainties to improve the accuracy of position estimation. Besides, the SG and EXS parameters can be identified concurrently online by a multistage genetic algorithm-based measurement scheme proposed in [33]. Furthermore, with the purpose of overcoming the difficulty in conventional parameter identification method when the saturation effect is presented, based on $d-q$ axes tests, both the accuracy and precision of SG parameter estimation are improved with the saturation effect taken into consideration [34]. Nevertheless, the single-machine infinite bus system is usually utilized for verifying various methods, which is not fully adaptable for a DFIM-SPS. The effects of parameter deviations of PGU on the performance of DFIM-SPS needs to be further investigated as the partially power decoupled system architecture cannot be equivalent to a general case of infinite grid.

This paper first explains the detailed models of SG and its EXS, and then up to 40% of parameter deviations are presented in the 16 key PGU parameters for a DFIM-SPS in the high-speed operation mode. The DFIM is modelled by regarding the two input electrical ports as a synthetic internal voltage [35, 36], and the control effects of phase-locked loop (PLL) fade away by using a novel vector control method. The parameter deviation effects for 16 PGU parameters on the terminal voltage and active power output are extensively studied with respect to the variations in three parameter deviation effect indicators (PDEIs) when different degrees of parameter deviations are applied. Finally, after the two most influential PGU parameters are identified, the performance of DFIM-SPS by applying the proposed novel control method is evaluated for the cases with different degrees of parameter deviations for these two parameters.

The parameter deviation effects in the PGU of DFIM-SPS are extensively investigated from different aspects by defining three PDEIs, which provides a promising way of evaluating the system performance. In addition, the most influential PGU parameters on affecting the system performance are identified, which is of paramount importance for properly designing the key system parameters to avoid unstable system operation.
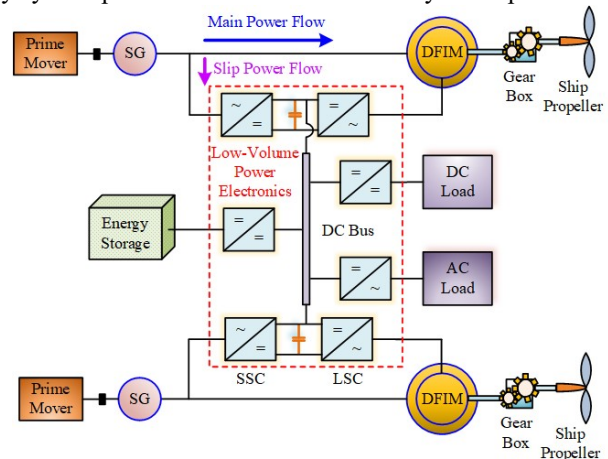

Fig. 1. The system structure of DFIM-SPS.

NI et al. : PARAMETER DEVIATION EFFECT STUDY OF THE POWER GENERATION UNIT ON A DOUBLY-FED INDUCTION MACHINE-BASED SHIPBOARD PROPULSION SYSTEM

341

The paper is organized in the following structure: In Section II, DFIM-SPS modelling is illustrated. In Section III, the novel vector control strategy is described. Then, three PDEIs are developed to analyze the DFIM-SPS performance affected by parameter deviations of PGU parameters. In Section V, simulation results are displayed. Finally, Section VI presents the conclusion.

II. MODELLING OF DFIM-SPS

The basic power components in a set of DFIM-SPS contain an internal combustion engine, an SG with EXS, and a DFIM with BTB power converter connected between its stator and rotor sides. The BTBPC includes the source side converter (SSC) and load side converter (LSC), and they are employed to control the DC-bus voltage and operation of DFIM, respectively. Fig. 1 shows the system structure of DFIM-SPS.

A. Standard Synchronous Generator

In this paper, a PGU consisting of a salient-pole SG and a type DC1A EXS functions as the power supplier for DFIM-SPS. The stator, field and damper windings of a salient-pole SG are taken into consideration, and the rotor parameters are equivalent to the stator side. The d-axis equivalent circuit contains both the field and damper windings, while there is no field winding in the q-axis one. The salient-pole SG dq equivalent circuit model is shown in Fig. 2.

The dq electrical model of a standard salient-pole SG can be expressed by the equations as shown below.

$$\begin{cases} \vec{v}_{dq} = R_{SG}\vec{i}_{dq} + p\vec{\psi}_{dq} + j\omega_{SG}\vec{\psi}_{dq} \\ v_{fd} = R_{fd}i_{fd} + p\psi_{fd} \\ \vec{v}_{kdq} = R_{kd}\vec{i}_{kdq} + p\vec{\psi}_{kdq} \end{cases} \quad (1)$$

$$\begin{cases} \psi_d = L_d i_d + L_{md}(i_{fd} + i_{kd}) \\ \psi_q = L_q i_q + L_{mq}i_{kq} \\ \psi_{fd} = L_{fd}i_{fd} + L_{md}(i_d + i_{kd}) \\ \psi_{kd} = L_{kd}i_{kd} + L_{md}(i_d + i_{fd}) \\ \psi_{kq} = L_{kq}i_{kq} + L_{mq}i_q \end{cases} \quad (2)$$

On the other hand, the mechanical behaviour is explained according to the following equations.

$$\Delta\omega_{SG}(t) = \frac{1}{2H}\int_0^t (T_m - T_{em})dt - K_d\Delta\omega_{SG}(t) \quad (3)$$

$$\omega_{SG}(t) = \Delta\omega_{SG}(t) + \omega_{SG0} \quad (4)$$

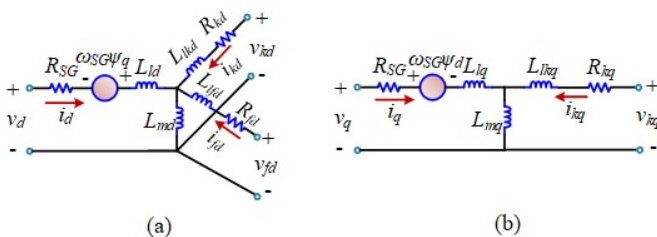The reactance values of SG in the dq reference frame are calculated as shown below.

Fig. 2. SG electrical model in dq frame (a) d-axis (b) q-axis

$$\begin{cases} X_d = X_{ld} + X_{md} \\ X_d{}' = X_{ld} + (X_{md} \| X_{lf}) \\ X_d{}'' = X_{ld} + (X_{md} \| X_{lf} \| X_{lkd}) \\ X_q = X_{lq} + X_{mq} \\ X_q{}'' = X_{lq} + (X_{mq} \| X_{lkq}) \end{cases} \quad (5)$$

B. EXS

The EXS is made up of an exciter, a terminal voltage transducer and load compensator, excitation control elements, and a power system stabilizer and the supplementary discontinuous excitation controls [37].

The inputs for the excitation control elements include the reference, stabilizing and compensating voltages, and the over and under excitation limiters are presented to implement saturations. The exciter is employed to produce the field voltage for the SG. Meanwhile, the voltage sensing and compensation are realized by using the load compensator and terminal voltage transducer, respectively. Additionally, the stabilizing function can be obtained by power system stabilizer and supplementary discontinuous excitation controls.

C. DFIM

DFIM is a type of induction machine with wound rotor windings, and the electromechanical energy conversion is realized by energizing both the stator and rotor circuits. With such a configuration, there is a wide speed range for the SPS when the ship runs at a high speed, and the strong overload capability is presented. The dq electrical model of DFIM is shown as follows.

$$\begin{cases} \vec{v}_{sdq} = R_s\vec{i}_{sdq} + p\vec{\varphi}_{sdq} + j\omega_e\vec{\psi}_{sdq} \\ \vec{v}_{rdq} = R_r\vec{i}_{rdq} + p\vec{\varphi}_{rdq} + j(\omega_e - \omega_r)\vec{\psi}_{rdq} \end{cases} \quad (6)$$

$$\begin{cases} \vec{\psi}_{sdq} = L_{ls}\vec{i}_{sdq} + L_m(\vec{i}_{sdq} + \vec{i}_{rdq}) \\ \vec{\psi}_{rdq} = L_{lr}\vec{i}_{rdq} + L_m(\vec{i}_{sdq} + \vec{i}_{rdq}) \end{cases} \quad (7)$$

The expressions of the electromagnetic torque T_{em} and the mechanical rotor speed ω_m are

$$T_{em} = 1.5n_p L_m(i_{rd}i_{sq} - i_{rq}i_{sd}) \quad (8)$$

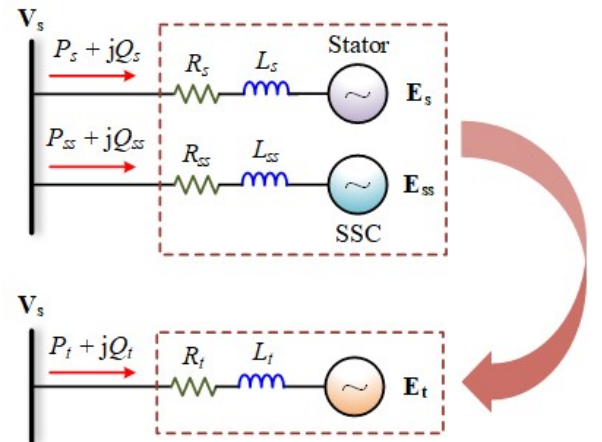$$\omega_m(t) = \frac{1}{2H}\int_0^t (T_{em} - T_L)dt + \omega_{m0} \quad (9)$$

Fig. 3. The equivalent circuit of the two electrical input ports for DFIM-SPS

DFIM is an induction machine with two electrical input ports and one mechanical output port. The two input ports can be characterized as two internal voltages for the stator and SSC terminals, E_s and E_{ss}, respectively [35, 36]. For the convenience of analyzing the system, the equivalent internal voltage for the whole DFIM-SPS can be derived, whose equivalent impedance is calculated by

$$R_t + j\omega_e L_t = \frac{1}{1/(R_s + j\omega_e L_s) + 1/(R_{ss} + j\omega_e L_{ss})} \quad (10)$$

The stator and SSC side electrical input ports are presented for DFIM-SPS in Fig. 3. According to Fig. 3, and by substituting (10) into (9), the dq components of the internal stator voltage of DFIM is expressed as

$$\vec{E}_{sdq} = \vec{v}_{sdq} - R_s \vec{i}_{sdq} - pL_s \vec{i}_{sdq} + j\omega_e L_s \vec{i}_{sdq} \quad (11)$$

Comparing (11) with (6) and (7), the expressions of E_{sd} and E_{sq} are modified as

$$\vec{E}_{sdq} = j\omega_e L_m \vec{i}_{rdq} \quad (12)$$

D. Overall System Structure

The DFIM-SPS can then be represented by the combination of PGU and the equivalent internal voltages of the stator and SSC of DFIM, which can be replaced with the synthetic internal voltage E_t.

$$\vec{E}_t = \frac{R_{ss} + j\omega_e L_{ss}}{(R_s + j\omega_e L_s)(R_{ss} + j\omega_e L_{ss})} \vec{E}_s + \frac{R_s + j\omega_e L_s}{(R_s + j\omega_e L_s)(R_{ss} + j\omega_e L_{ss})} \vec{E}_{ss} \quad (13)$$

Substituting (10) into (13), expression for E_t is updated as

Fig. 4. The system under investigation

$$\vec{E}_t = \frac{R_t + j\omega_e L_t}{R_s + j\omega_e L_s} \vec{E}_s + \frac{R_t + j\omega_e L_t}{R_{ss} + j\omega_e L_{ss}} \vec{E}_{ss} \quad (14)$$

By neglecting the resistances, (14) can be simplified as

$$\vec{E}_t = L_t[(1/L_s)\vec{E}_s + (1/L_{ss})\vec{E}_{ss}] \quad (15)$$

By replacing the two electrical ports with the synthetic internal voltage E_t, the system under investigation is derived as shown in Fig. 4.

III. Control of DFIM-SPS

A. Type DC1A EXS

As the type DC1A EXS is widely used in industry, it is taken as the one used in the proposed DFIM-SPS in this paper. The amplitude of the SG stator voltages is obtained through a low-pass filter (LPF), which is also the terminal voltage V_T. The other three inputs to the EXS are the reference voltage V_{ref}, stabilizing voltage V_{stab} and initial field voltage V_{f0}. The control signal is produced through the use of a first-order automatic voltage regulator (AVR), after which an exciter is applied to

Fig. 5. Field voltage control logic by DC1A EXS

generate the field voltage V_f. To keep the system stable, a stabilizer is employed to feed the field voltage signal back. The corresponding control block diagram is displayed in Fig. 5.

B. DFIM

For a DFIM-SPS, the PGU consisting of an SG and its EXS provides power to the propulsion load, and the PGU parameter changes can directly affect the system operation. Usually the stator resistance of DFIM is small enough to be neglected. In this case, the PLL can be eliminated to avoid possible system performance deterioration caused by improper controller parameter design, and the synchronous angle can be estimated based on the flux angle θ_φ. Therefore, the DFIM vector control structure can be simplified, which is displayed in Fig. 6.

A steady DC-bus voltage and sinusoidal three-phase input current waveforms are to be achieved by the control of SSC. The DC-bus voltage can be calculated according to the difference between the SSC input active power P_{ss} and the LSC output active power P_r. The DC-link voltage dynamics are

$$V_{dc} = \sqrt{\frac{2(P_{ss} - P_r)}{sC_{dc}}} \quad (16)$$

$$i_{ssdref} = (V_{dcref} - V_{dc})(k_{p1} + k_{i1}/s) \quad (17)$$

For LSC, the electromagnetic torque is controlled by controlling the d-axis rotor current, while the stator reactive power is controlled based on the control of q-axis rotor current. The rotor dq current reference values are obtained by

$$i_{rdref} = \frac{(\omega_m - \omega_{mref})(k_{p3} + k_{i3}/s)}{k_s |\varphi_s|} \quad (18)$$

Fig. 6. Vector control of DFIM-SPS with PLL elimination

$$i_{rqref} = (V_{sref} - V_s)(k_{p4} + k_{i4}/s) \quad (19)$$

Where $k_s = L_m/L_s$ is the stator coupling factor.

IV. PARAMETER DEVIATION EFFECT INDICATORS FOR THE SYSTEM

The accuracy of PGU parameters is of paramount importance for the steady and reliable operation of DFIM-SPS. However, variations in theses parameters are inevitable in practice. In this section, 16 important parameters for SG (X_d, X_d', X_d'', X_q, X_q'', X_l, T_{do}', T_{do}'' and T_{qo}'') and its EXS (K_a, T_a, K_e, T_e, K_f, T_f, T_r) are taken into account. The effects on the output terminal voltage V_T and active power P_e of SG are studied by applying different degrees of parameter deviations for each parameter. Since the input to SG is the rotor angular speed, there is no need to define the inertia and friction factor. In addition, the rotor type of the applied SG is salient-pole, under which circumstance the q-axis transient reactance X_q' is not available. The PGU parameter values are displayed in Appendix.

In order to evaluate the parameter deviation effects on the system performance from different aspects, three parameter deviation effect indicators (PDEIs) are developed.

The average error between the output signal value (*OSV*) with parameter deviations and that without parameter deviation is evaluated by the average deviation (*AVGD*).

$$AVGD = \frac{1}{N}\sum_{i=1}^{N}(OSV_i - OSV_{iPD}) \quad (20)$$

where N represents the number of sampling points, i indicates the ith sampling point, and iPD indicates the value with parameter deviation at the ith sampling point.

Besides, the overall deviation of *OSV* can be measured by applying the concept of standard deviation (*STDEV*) by covering the whole sampling period, where the dispersion degree of samples is derived for each parameter.

$$STDEV = \sqrt{\frac{1}{N}\sum_{i=1}^{N}[(OSV_i - OSV_{iPD}) - AVGD]^2} \quad (21)$$

Moreover, for the sake of revealing the absolute error between the values of *OSV* with and without parameter deviation, the average square root of quadratic sum (*ASRQS*) can be applied as it has a positive correlation with the absolute error.

$$ASRQS = \frac{1}{N}\sqrt{\sum_{i=1}^{N}(OSV_i - OSV_{iPD})^2} \quad (22)$$

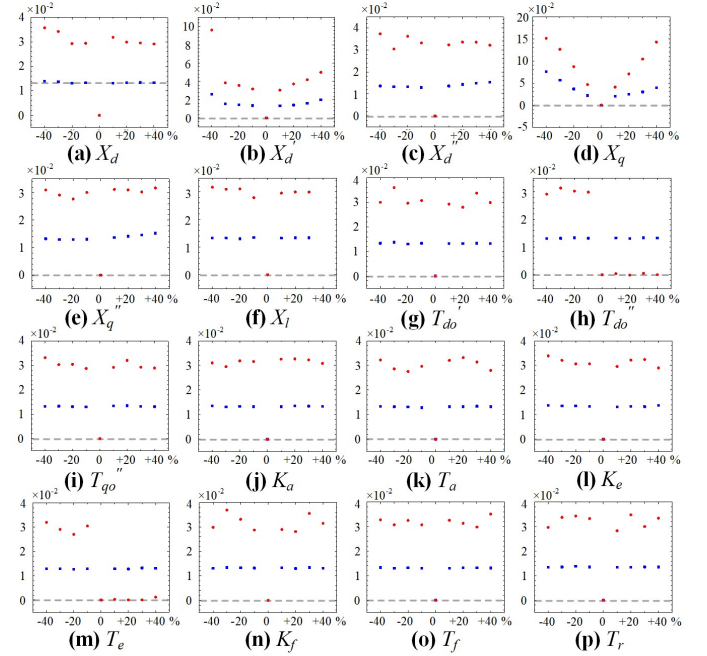In this paper, *OSV* represents V_T or P_e.

Fig. 8. *STDEV* for different degrees of parameter deviations of the 16 PGU parameters for V_T and P_e

Fig. 7. *AVGD* for different degrees of parameter deviations of the 16 PGU parameters for V_T and P_e
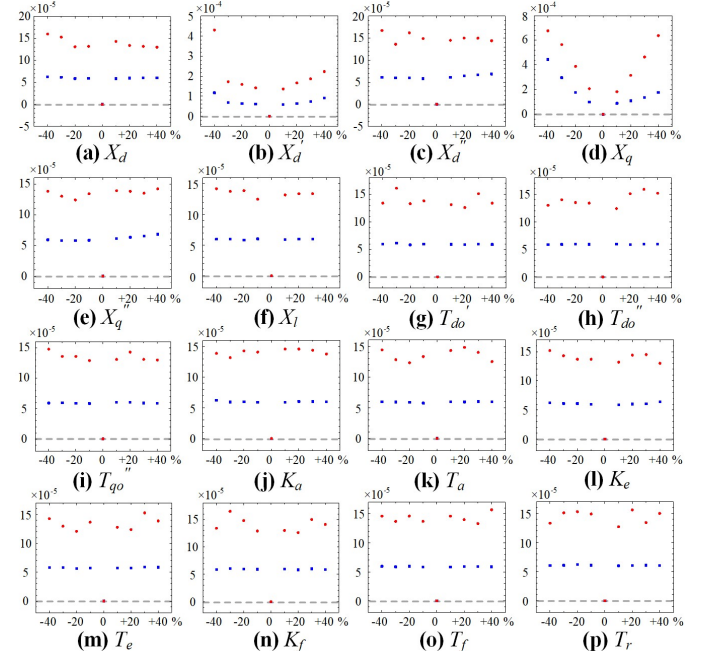

Fig. 9. *ASRQS* for different degrees of parameter deviations of the 16 PGU parameters for V_T and P_e

V. SIMULATION RESULTS AND DISCUSSION

The DFIM-SPS discrete model with the time step of 5μs is simulated in Matlab/Simulink to investigate its operation with parameter deviations in the PGU. Since the transmission lines for the SPS are much shorter than those of a grid connected power system, the impedances of transmission lines are neglected, and the transformer impedance Z_{tr} is also set to 0. The details of system parameters are shown in Appendix.
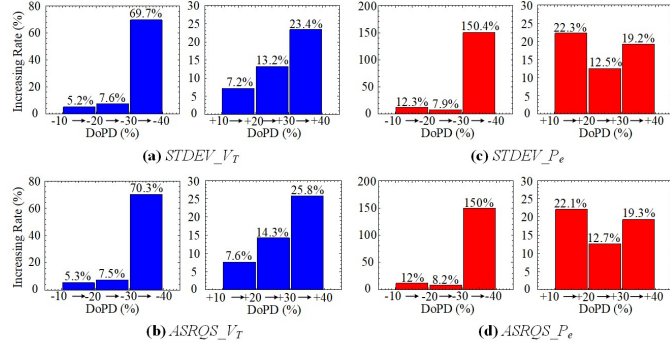

Fig. 10. PDEI increasing rates with respect to degree of parameter deviation variations of X_d'
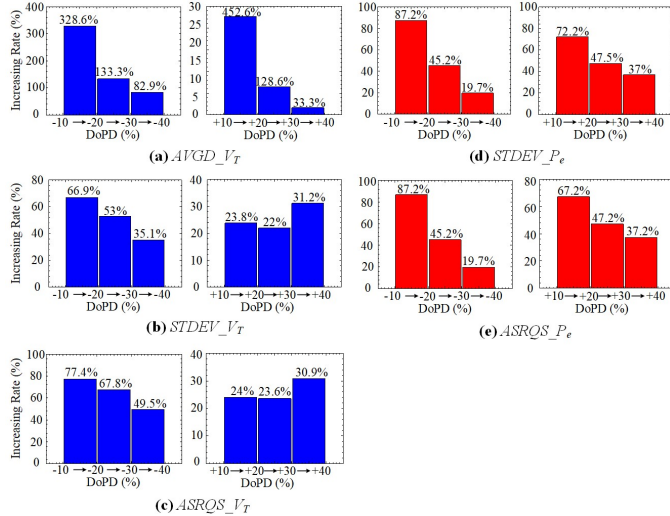
Fig. 11. PDEI increasing rates with respect to degree of parameter deviation variations of X_q
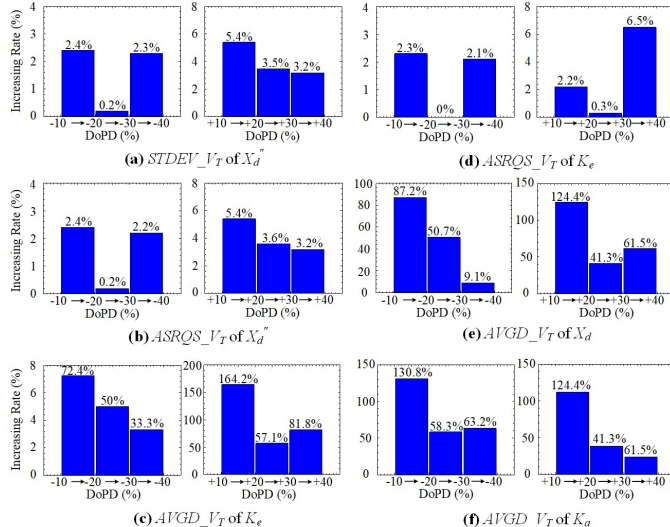
Fig. 12. PDEI increasing rates with respect to degree of parameter deviation variations of X_d'', K_e, X_d and K_a

With all the three aforementioned PDEIs, the parameter deviation effects can be studied roundly. The values of *AVGD*, *STDEV* and *ASRQS* for V_T and P_e in the cases of applying different degrees of parameter deviations for PGU are displayed in Figs. 7-9. The PDEI values for V_T and P_e are indicated by blue squares and red dots, respectively, and they are all in the unit of pu.

The degrees of parameter deviations for each parameter are set as -40%, -30%, -20%, -10%, +10%, +20%, +30% and +40% respectively from the actual value to study the parameter deviation effects on two output variables V_T and P_e. It can be seen from Figs. 7-9 that varying the degree of parameter deviations of X_d' and X_q affects the values of PDEIs for V_T and P_e significantly, and the degrees of parameter deviations of X_d'' and K_e majorly relate to the variations of PDEIs for V_T. In addition, the values of *AVGD* for V_T obviously change with the variations of degree of parameter deviations in X_d and K_a. Nevertheless, parameter deviations in the other parameters hardly influence the SG output performance. Therefore, the key parameters to be further discussed are X_d', X_q, X_d'', K_e, X_d and K_a. Moreover, the effects of parameter deviations on P_e are generally more significant than those on V_T, as can be seen from most diagrams in Figs. 7-9.
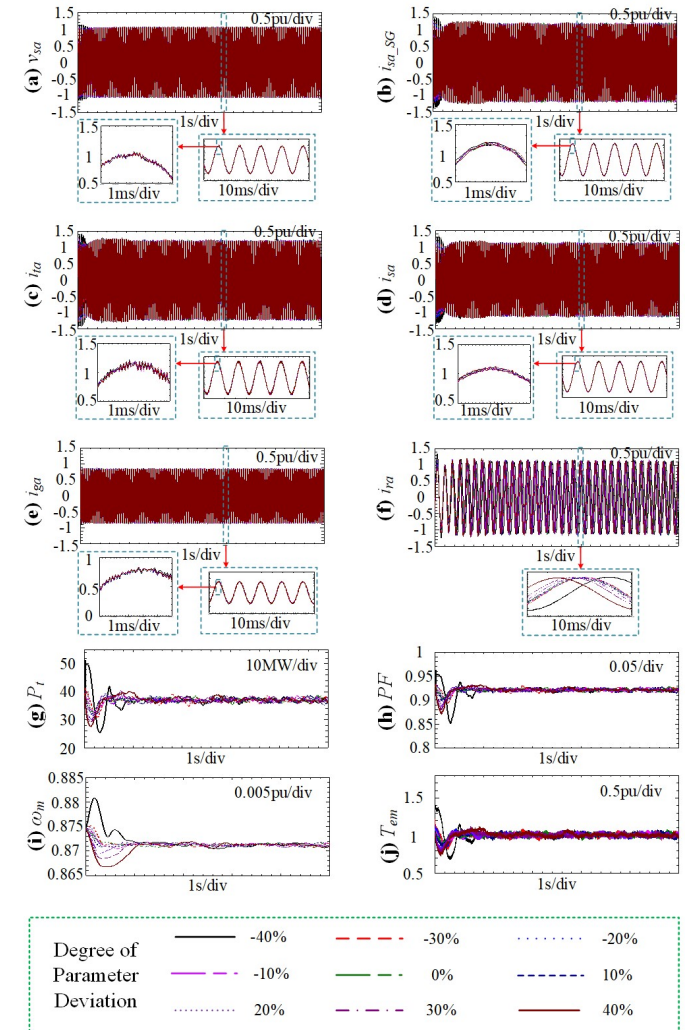

Fig. 13. Simulation results of DFIM-SPS with different degrees of parameter deviations for X_d'

NI et al. : PARAMETER DEVIATION EFFECT STUDY OF THE POWER GENERATION UNIT ON A DOUBLY-FED INDUCTION MACHINE-BASED SHIPBOARD PROPULSION SYSTEM

345

The parameter deviations of X_d' obviously influence *STDEV* and *ASRQS* for both V_T and P_e of SG. When applying different degrees of parameter deviations for X_q, *AVGD* for V_T is also significantly affected. In addition, the parameters X_d'', K_e, X_d and K_a only have obvious impacts on the increasing rates of some PDEIs for V_T when the degree of parameter deviation varies. By increasing the degree of parameter deviation in either the negative or positive way, the increasing rates of these PDEIs vary for different regions of degree of parameter deviation variations for each parameter. In order to analyse the phenomenon in detail, the increasing rates of PDEIs with respect to degree of parameter deviation variations of X_d', X_q, X_d'', K_e, X_d and K_a are shown in Figs. 10 – 12, respectively.

According to the bar graphs in Fig. 10, with the increase of degree of parameter deviation of X_d', the increasing rates of *STDEV* and *ASRQS* for V_T keep rising, while those in the variation regions of (-20%) to (-30%) and (+20%) to (+30%) are the lowest ones for P_e. Additionally, the increasing rates in the variations regions of (-30%) to (-40%) are much higher than the others for both the cases of PDEIs for V_T and P_e. In terms of X_q, the increasing rates keep falling for all the PDEIs shown in Fig. 11 except the positive variation directions for *STDEV* and

ASRQS for V_T. Besides, the increasing rates of *AVGD* for V_T are astonishingly high for the variation regions of (-10%) to (-20%) and (+10%) to (+20%). Therefore, it can be deduced that the system performance will be significantly affected even if a slight degree of parameter deviation is applied to X_q.

From Fig. 12, it can be seen that changing the degree of parameter deviation of X_d'' has little impact on the increasing rates of the corresponding PDEIs. In addition, in spite of a slightly high increasing rate (6.5%) in the region of (+30%) to (+40%) for the degree of parameter deviation of K_e in the case of *ASRQS* for V_T, the overall impact of degree of parameter deviation of K_e on the PDEI is negligible. The trends of increasing rate variation are the same for *AVGD* for V_T of K_e and X_d, and the highest values appear in the regions that are closest to the points of actual values, which is also the case for *AVGD* for V_T of K_a. Therefore, the deviations of V_T from the actual value will be obvious when applying a small degree of parameter deviation for K_e, X_d and K_a.

Since the DPs of X_d' and X_q play the most important role in affecting the output voltage and active power of SG, the system performance is strongly related to the degrees of parameter deviations of these two parameters. The simulation results of key system variables in the proposed DFIM-SPS are obtained when applying different degrees of parameter deviations for X_d' and X_q, which are displayed in Figs. 13 and 14, respectively. The SG variables are endowed with the subscript "_SG", while the others correspond to the DFIM variables.

In this section, the waveforms of phase-A voltage and current are displayed as representatives for the three-phase system. From Fig. 13(a), the phase-A stator voltages derived by applying different degrees of parameter deviations almost coincide with each other. However, fluctuations in the values are presented, and the larger the fluctuations are, the larger the degrees of parameter deviations are. As a result, the current waveforms also have the similar performance, which are shown in Fig. 13(b) – (e). Since the three-phase rotor currents are with a low frequency, obvious deviations of i_{ra} with 40% degree of parameter deviation (either positive or negative) from those with other values are presented. From Figs. 13(g) and (h), the oscillations of P_t and PF can be clearly observed at the beginning for the cases with large degrees of parameter deviations, while their values with different degrees of parameter deviations converge as time goes by. The situations are similar for the DFIM rotor speed ω_m and electromagnetic torque T_{em}, which are shown in Figs. 13(i) and (j).

Different from the simulation results in Fig. 13, what is observed from Fig. 14 is that the phase-A voltage and current waveforms with different degrees of parameter deviations distinctly deviate from each other, as the degree of parameter deviation of X_q is positively correlated with *AVGD* for V_T. On top of that, the oscillations in the total active power P_t, power factor PF, rotor speed ω_m and electromagnetic torque T_{em} are much larger than those in the previous case for each degree of parameter deviation. Moreover, the settling time for ω_m and T_{em} is much longer. Therefore, the simulation results in Fig. 14 cater to the descriptions for Figs. 7-12.
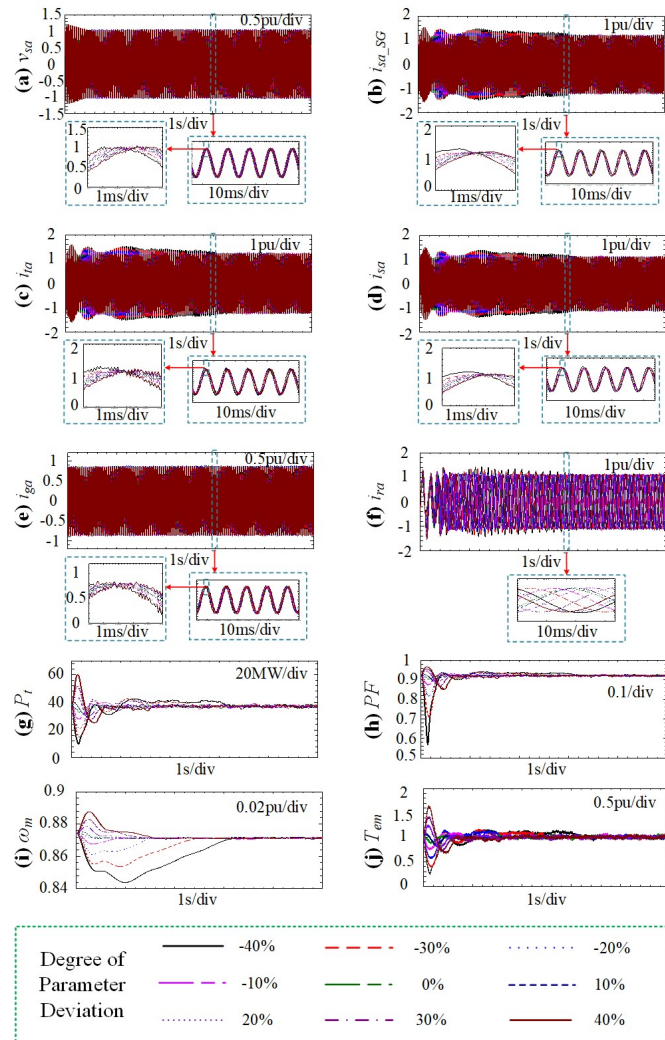

Fig. 14. Simulation results of DFIM-SPS with different degrees of parameter deviations for X_q

VI. Conclusion

The parameter deviation effects of PGU on a partially power decoupled DFIM-SPS is investigated in this paper. The modelling and control of a DFIM-SPS are studied in detail. The system performance affected by parameter deviation effects are evaluated according to three PDEIs for different degrees of parameter deviations for a specific parameter. In this paper, 16 important SG and EXS parameters are taken for sensitivity analysis to study the parameter deviation effects on terminal voltage and output active power. The overall system performance is further investigated for the two most influential PGU parameters, which are X_d' and X_q. According to the simulation results, the following points are obtained to conclude the vital clues on PGU parameter identification for a DFIM-SPS.

(1) The parameter deviations of X_d' and X_q affect almost all the PDEIs for V_T and P_e significantly, except $AVGD$ in the cases of X_d' and P_e for X_q.

(2) The parameter deviations of X_d'', K_e, X_d and K_a have considerable influence on some of the PDEIs for V_T.

(3) The effects of parameter deviations on P_e are generally more significant than those on V_T.

(4) A slight degree of parameter deviation of X_q can significantly affect the system performance, as the increasing rate of $AVGD$ for V_T when applying a small degree of parameter deviation for X_q is extremely high.

(5) Obvious deviations of V_T from the actual value can be expected when small degrees of parameter deviations for K_e, X_d and K_a are applied.

(6) There is no obvious deviation for the three-phase voltages and currents when applying different degrees of parameter deviations for X_d', and P_t, PF, ω_m and T_{em} can converge with few oscillations.

(7) The deviations and oscillations in the corresponding variables for a specific degree of parameter deviation are much larger for the case of X_q than that of X_d', and it takes longer for ω_m and T_{em} to be stable.

Overall, the degrees of parameter deviations of the d-axis transient reactance and q-axis reactance of SG X_d' and X_q have the most obvious positive relations with the three PDEIs. Furthermore, the parameter deviations of X_q have the most significant impacts on the system performance of DFIM-SPS. Therefore, it is necessary to precisely identify the value of X_q to ensure the system stability.

Appendix

A. System Parameters of DFIM-SPS

P_n = 36MW; V_{nSG} = 13.8kV; V_n = 4.16kV; f_n = 50Hz; C_{dc} = 10mF; R_{SG} = 0.036pu; n_{pSG} = 20; R_s = 0.023pu; L_{ls} = 0.18pu; R_r = 0.016pu; L_{lr} = 0.16pu; L_m = 2.9pu; H = 3.5s; n_p = 3; R_{ss} = 0.003pu; L_{ss} = 0.3pu; F = 0.01pu.

B. System Parameters of PGU

X_d = 1.321pu; X_d' = 0.1685pu; X_d'' = 0.105pu; X_q = 1.173pu; X_q'' = 0.09pu; X_l = 0.075pu; T_{do}' = 6.5s; T_{do}'' = 0.0241s; T_{qo}'' = 0.0464s; K_a = 300; T_a = 0.001s; K_e = 1; T_e = 0.0001s; K_f = 0.0001; T_f = 0.1s; T_r = 0.02s.

References

[1] F. Wang, Z. Zhang, T. Ericsen, R. Raju, R. Burgos, and D. Boroyevich, "Advances in Power Conversion and Drives for Shipboard Systems," *Proceedings of the IEEE,* vol. 103, no. 12, pp. 2285-2311, Dec. 2015.

[2] Z. Jin, G. Sulligoi, R. Cuzner, L. Meng, J. C. Vasquez, and J. M. Guerrero, "Next-Generation Shipboard DC Power System: Introduction Smart Grid and dc Microgrid Technologies into Maritime Electrical Netowrks," *IEEE Electr. Magn.,* vol. 4, no. 2, pp. 45-57, Jun. 2016.

[3] Z. Jin, L. Meng, J. M. Guerrero, and R. Han, "Hierarchical Control Design for a Shipboard Power System With DC Distribution and Energy Storage Aboard Future More-Electric Ships," *IEEE Trans. Ind. Informat.,* vol. 14, no. 2, pp. 703-714, Feb. 2018.

[4] *IEEE recommended practice for 1 to 35kV medium voltage DC power systems on ships.*, 2010.

[5] S. Yang, D. Xiang, A. Bryant, P. Mawby, L. Ran, and P. Tavner, "Condition Monitoring for Device Reliability in Power Electronic Converters: A Review," *IEEE Trans. Power Electron.,* vol. 25, no. 11, pp. 2734-2752, Nov. 2010.

[6] P. Cairoli and R. A. Dougal, "Fault Detection and Isolation in Medium-Voltage DC Microgrids: Coordination Between Supply Power Converters and Bus Contactors," *IEEE Trans. Power Electron.,* vol. 33, no. 5, pp. 4535-4546, May 2018.

[7] E. Christopher, M. Sumner, D. W. P. Thomas, X. Wang, and F. de Wildt, "Fault Location in a Zonal DC Marine Power System Using Active Impedance Estimation," *IEEE Trans. Ind. Appl.,* vol. 49, no. 2, pp. 860-865, Mar./Apr. 2013.

[8] K. Satpathi, A. Ukil, and J. Pou, "Short-Circuit Fault Management in DC Electric Ship Propulsion System: Protection Requirements, Review of Existing Technologies and Future Research Trends," *IEEE Trans. Transport. Electrific.,* vol. 4, no. 1, pp. 272-291, Mar. 2018.

[9] C. Gong, Y. Hu, G. Chen, H. Wen, Z. Wang, and K. Ni, "A DC-Bus Capacitor Discharge Strategy for PMSM Drive System With Large Inertia and Small System Safe Current in EVs," *IEEE Trans. Ind. Informat.,* vol. 15, no. 8, pp. 4709-4718, Aug. 2019.

[10] C. Gan, Q. Sun, J. Wu, W. Kong, C. Shi, and Y. Hu, "MMC-Based SRM Drives With Decentralized Battery Energy Storage System for Hybrid Electric Vehicles," *IEEE Trans. Power Electron.,* vol. 34, no. 3, pp. 2608-2621, Mar. 2019.

[11] Z. Yu, C. Gan, Y. Chen, and R. Qu, "DC-biased Sinusoidal Current Excited Switched Reluctance Motor Drives Based on Flux Modulation Principle," *IEEE Trans. Power Electron.,* pp. 1-1, 2020.

[12] C. Gan, J. Wu, Y. Hu, S. Yang, W. Cao, and J. M. Guerrero, "New Integrated Multilevel Converter for Switched Reluctance Motor Drives in Plug-in Hybrid Electric Vehicles With Flexible Energy Conversion," *IEEE Trans. Power Electron.,* vol. 32, no. 5, pp. 3754-3766, May 2017.

[13] J. Hu, Y. Huang, D. Wang, H. Yuan, and X. Yuan, "Modeling of Grid-Connected DFIG-Based Wind Turbines for DC-Link Voltage Stability Analysis," *IEEE Trans. Sustain. Energy,* vol. 6, no. 4, pp. 1325-1336, Oct. 2015.

[14] N. E. Ouanjli *et al.*, "Modern improvement techniques of direct torque control for induction motor drives-a review," *Protection and Control of Modern Power Systems,* vol. 4, no. 2, pp. 136-147, 2019.

[15] C. Gong, Y. Hu, K. Ni, J. Liu, and J. Gao, "SM Load Torque Observer-Based FCS-MPDSC With Single Prediction Horizon for High Dynamics of Surface-Mounted PMSM," *IEEE Trans. Power Electron.,* vol. 35, no. 1, pp. 20-24, Jan. 2020.

[16] M. Cheng, P. Han, G. Buja, and M. G. Jovanovic, "Emerging Multiport Electrical Machines and Systems: Past Developments, Current Challenges, and Future Prospects," *IEEE Transactions on Industrial Electronics,* vol. 65, no. 7, pp. 5422-5435, 2018.

[17] K. Ni, Y. Hu, C. Gan, C. Gong, and H. Wen, "Synthetic Internal Voltage Phase–Amplitude Dynamics Investigation for Electric Drivetrain Small-Signal Model in Electromechanical Control Timescale for a Wound Rotor Induction Machine-Based Shipboard Power System," *IEEE Trans. Transportation Electrific.,* vol. 6, no. 2, pp. 844-855, June 2020.

[18] K. Ni, Y. Hu, Z. Wang, H. Wen, and C. Gan, "Asynchronized Synchronous Motor-Based More Electric Ship—Less Power Electronics for More System Reliability," *IEEE/ASME Trans. Mechatron.,* vol. 24, no. 5, pp. 2353-2364, Oct. 2019.

[19] G. Poddar and V. T. Ranganathan, "Direct Torque and Frequency Control of Double-Inverter-Fed Slip-Ring Induction Motor Drive," *IEEE*

NI et al.: PARAMETER DEVIATION EFFECT STUDY OF THE POWER GENERATION UNIT ON A DOUBLY-FED INDUCTION MACHINE-BASED SHIPBOARD PROPULSION SYSTEM

347

Transactions on Industrial Electronics, vol. 51, no. 6, pp. 1329-1337, 2004.

[20] F. Bonnet, P. E. Vidal, and M. Pietrzak-David, "Dual Direct Torque Control of Doubly Fed Induction Machine," *IEEE Transactions on Industrial Electronics,* vol. 54, no. 5, pp. 2482-2490, 2007.

[21] K. Chen, P. Delarue, A. Bouscayrol, P.-E. Vidal, and M. Pietrzak-David, "Minimum Copper Loss and Power Distribution Control Strategies of Double-Inverter-Fed Wound-Rotor Induction Machines Using Energetic Macroscopic Representation," *IEEE Transactions on Energy Conversion,* vol. 25, no. 3, pp. 642-651, 2010.

[22] Y. Liu and L. Xu, "The Dual-Current-Loop Controlled Doubly Fed Induction Motor for EV/HEV Applications," *IEEE Transactions on Energy Conversion,* vol. 28, no. 4, pp. 1045-1052, 2013.

[23] A. Banerjee, M. S. Tomovich, S. B. Leeb, and J. L. Kirtley, "Power Converter Sizing for a Switched Doubly Fed Machine Propulsion Drive," *IEEE Transactions on Industry Applications,* vol. 51, no. 1, pp. 248-258, 2015.

[24] A. Banerjee, M. S. Tomovich, S. B. Leeb, and J. L. Kirtley, "Control Architecture for a Switched Doubly Fed Machine Propulsion Drive," *IEEE Transactions on Industry Applications,* vol. 51, no. 2, pp. 1538-1550, 2015.

[25] F. P. DEMELLO and C. CONCORDIA, "Concepts of Synchronous Machine Stability as Affected by Excitation Control," *IEEE Trans. Power App. Syst.,* vol. PAS-88, no. 4, pp. 316-329, Apr. 1969.

[26] I. M. Canay, "I.M. Canay_Determination of model parameters of synchronous machines," *IEE Proceedings,* vol. 130, no. 2, pp. 86-94, Mar. 1983.

[27] J. Tamura and I. Takede, "A NEW MODEL OF SATURATED SYNCHRONOUS MACHINES FOR POWER SYSTEM TRANSIENT STABILITY SIMULATIONS," *IEEE Trans. Energy Convers.,* vol. 10, no. 2, pp. 218-224, Jun. 1995.

[28] J. A. Martinez, B. Johnson, and C. Grande-Moran, "Parameter Determination for Modeling System Transients—Part IV: Rotating Machines," *IEEE Trans. Power Del.,* vol. 20, no. 3, pp. 2063-2072, 2005.

[29] L. Wang, J. Jatskevich, and H. W. Dommel, "Re-examination of Synchronous Machine Modeling Techniques for Electromagnetic Transient Simulations," *IEEE Trans. Power Syst.,* vol. 22, no. 3, pp. 1221-1230, Aug. 2007.

[30] M. Giuseppe Fusco and M. Russo, "Adaptive Voltage Regulator Design for Synchronous Generator," *IEEE Trans. Energy Convers.,* vol. 23, no. 3, pp. 946-956, Sep. 2008.

[31] H. Lomei, D. Sutanto, K. M. Muttaqi, and A. Alfi, "An Optimal Robust Excitation Controller Design Considering the Uncertainties in the Exciter Parameters," *IEEE Trans. Power Syst.,* vol. 32, no. 6, pp. 4171-4179, Nov. 2017.

[32] C. Gan, F. Meng, Z. Yu, R. Qu, Z. Liu, and J. Si, "Online Calibration of Sensorless Position Estimation for Switched Reluctance Motors With Parametric Uncertainties," *IEEE Trans. Power Electron.,* vol. 35, no. 11, pp. 12307-12320, Nov. 2020.

[33] B. Zaker, G. B. Gharehpetian, M. Karrari, and N. Moaddabi, "Simultaneous Parameter Identification of Synchronous Generator and Excitation System Using Online Measurements," *IEEE Trans. Smart Grid,* vol. 7, no. 3, pp. 1230-1238, May 2016.

[34] B. Zaker, G. B. Gharehpetian, and M. Karrari, "Improving Synchronous Generator Parameters Estimation Using d − q Axes Tests and Considering Saturation Effect," *IEEE Trans. Ind. Informat.,* vol. 14, no. 5, pp. 1898-1908, May 2018.

[35] J. Hu, H. Yuan, and X. Yuan, "Modeling of DFIG-Based WTs for Small-Signal Stability Analysis in DVC Timescale in Power Electronized Power Systems," *IEEE Trans. Energy Convers.,* vol. 32, no. 3, pp. 1151-1165, Sep. 2017.

[36] M. Zhao, X. Yuan, and J. Hu, "Modeling of DFIG Wind Turbine Based on Internal Voltage Motion Equation in Power Systems Phase-Amplitude Dynamics Analysis," *IEEE Trans. Power Syst.,* vol. 33, no. 2, pp. 1484-1495, Mar. 2018.

[37] *IEEE Recommended Practice for Excitation System Models for Power System Stability Studies,* 1992.

Kai Ni (S'17-M'20) was born in Jiangsu, China. He received the B.Eng. (Hons) degree and Ph.D. degree in Electrical Engineering from the University of Liverpool, Liverpool, UK, in 2016 and 2019, respectively. After obtaining the support from the Postdoctoral International Exchange Program, he joined the School of Electrical and Electronic Engineering at Huazhong University of Science and Technology from Dec. 2019 as a postdoctoral researcher. His research interests include modelling, control and stability analysis of doubly-fed induction machines, power electronic converters, and aircraft/shipboard power systems.

Dr. Ni was the recipient of the 2019 Chinese Government Award for Outstanding Self-financed Students Abroad.

Yihua Hu (M'13-SM'15) received the B.S. degree in electrical engineering in 2003, and the Ph.D. degree in power electronics and drives in 2011, both at China University of Mining and Technology. Between 2011 and 2013, he was with the College of Electrical Engineering, Zhejiang University as a Postdoctoral Fellow. Between 2013 and 2015, he worked as a Research Associate at the power electronics and motor drive group, the University of Strathclyde. Between 2016 and 2019, he was a Lecturer at the Department of Electrical Engineering and Electronics, University of Liverpool (UoL). Currently, he is a Reader at Electronics Engineering Department at The University of York (UoY). His research interests include renewable generation, power electronics converters & control, electric vehicle, more electric ship/aircraft, smart energy system and non-destructive test technology. He is the associate editor of IEEE Transactions on Industrial Electronics, IET Renewable Power Generation, IET Intelligent Transport Systems and Power Electronics and Drives.

Chun Gan (M'14) received the B.S. and M.S. degrees in electrical engineering from China University of Mining and Technology, Jiangsu, China, in 2009 and 2012, respectively, and the Ph.D. degree in electrical engineering and motor drives from Zhejiang University, Hangzhou, China, in 2016.

He is currently a Professor with the School of Electrical and Electronic Engineering, Huazhong University of Science and Technology, Wuhan, China. From 2016 to 2018, he was a Research Associate with the Department of Electrical Engineering and Computer Science,

University of Tennessee, Knoxville, TN, USA. He has authored/coauthored more than 80 peer-reviewed technical papers, including more than 50 IEEE Transaction papers. He has over 20 issued/published invention patents. His research interests include electrical motor drives, electrical motor converters, motor design, electric vehicles, electrified transportation, and high-efficiency power converters.

Dr. Gan was the recipient of the 2018 Highlighted Paper Award from IEEE TPEL, the 2018 Marie Sklodowska-Curie Actions Seal of Excellence Award from European Commission, and the 2019 Best Paper Award from ICEMS.